Hydrogen Confinement in Hexagonal Boron Nitride Bubbles Using UV Laser Illumination

Fatima Z Tijent, M.-B. Bouzourâa, Vishnu Ottapilakkal, Andre Perepeliuc, Rajat Gujrati, Phuong Vuong, Suresh Sundaram, Mustapha Faqir, Paul L Voss, Jean-Paul Salvestrini, et al.

Hydrogen Confinement in Hexagonal Boron Nitride Bubbles Using UV Laser Illumination

Fatima Z. Tijent*[1,2,3], Montassar B. Bouzourâa[4], Vishnu Ottapilakkal[1], Andre Perepeliuc[1,2], Rajat Gujrati[1], Phuong Vuong[1], Suresh Sundaram[1,2], Mustapha Faqir[5], Paul L. Voss[1,2], Jean-Paul Salvestrini[1,2] and Abdallah Ougazzaden[1,2]

**Corresponding author, E-mail address: ftijent3@gatech.edu*

[1]*CNRS, Georgia Tech – CNRS IRL 2958, 2 rue Marconi, 57070 Metz, France*

[2]*Georgia Institute of Technology, School of Electrical and Computer Engineering, Atlanta, GA 30332-0250, USA*

[3]*Université Internationale de Rabat, Aerospace and Automotive Engineering School and LERMA Lab, Rabat-Sale, 11100, Sala Al Jadida, Morocco*

[4]*Université de Lorraine, LCP-A2MC, F57000 Metz, France.*

[5]*Université Internationale de Rabat, Aerospace and Automotive Engineering School, Rabat-Sale, 11100, Sala Al Jadida, Morocco*

Abstract

Hexagonal boron nitride bubbles are of significant interest to micro-scale hydrogen storage thanks to their ability to confine hydrogen gas molecules. Previous reports of h-BN bubble creation from grown h-BN films require electron beams under vaccum, making integrating with other experimental setups for hydrogen production impractical. Therefore, in this study, we demonstrate the formation of h-BN bubbles in a 20 nm h-BN film grown on a sapphire substrate with a 213 nm UV laser beam. Using atomic force microscopy, we show that longer illumination time induces larger h-BN bubbles up to 20 μm with higher density. We also demonstrate that h-BN bubbles do not collapse for more than six months after their creation. We report the internal pressure and gravimetric storage capacity of h-BN bubbles. We obtained a maximum internal pressure of 41 MPa and a gravimetric storage capacity of 6 %. These findings show that h-BN bubbles can be a promising system for long-term hydrogen storage.

Keywords

Hydrogen gas, h-BN, UV laser, bubbles, hydrogen storage

1. Introduction

Hexagonal boron nitride (h-BN) has recently attracted interest in green hydrogen production and storage applications because of its unique properties [1–4]. h-BN has a high chemical resistance to oxidation, which makes it a promising corrosion inhibitor [1,2]. Furthermore, h-BN's 2D structure enables it to act as a proton exchange membrane and hydrogen storage system [3–5]. This is due to h-BN's nanopores, which allow easy diffusion of hydrogen protons while preventing the escape of hydrogen molecules [5]. Moreover, h-BN is more porous to hydrogen ions than graphene and MoS_2 [3,5–8] because of the uneven distribution of valence electrons. These electrons are more clustered around N atoms, reflecting the strong and polarized nature of B-N bonds. Additionally, bi- and tri-layered graphene are nonconductive to protons owing to their staggered lattices (AB stacking), in which the first layer's pores clog the second one's pores. On the contrary, multilayered h-BN exhibits good proton conductivity thanks to the AA' stacking structure [9].

In recent years, 2D material bubbles, including graphene, transition metal dichalcogenides (TMDs), and h-BN bubbles, have gained significant attention as proof-of-principle precursors for hydrogen gas storage applications. These bubbles facilitate the investigation and characterization of the confined hydrogen gas. In addition, they are highly strained, which alters the elastic, optical, and vibrational properties of the 2D material [10–12]. This finding is crucial as it can give rise to new micro-electronic systems with unique features. These bubbles can also provide a good platform for studying the adhesion energy between the 2D material and substrate [13].

Several approaches to creating 2D material bubbles have been reported. These bubbles can spontaneously be induced during the 2D material's transfer due to the adsorbed species on the 2D material surface or the substrate [13–16]. The size and shape of spontaneously induced bubbles are uncontrollable. 2D material bubbles can also be created using hydrogen proton irradiation [3,11,17]. In this approach, hydrogen protons penetrate the interlayers of 2D materials, where they recombine and form H_2-filled bubbles. The penetration depth of protons may differ from one material to another. An earlier study revealed that in h-BN nanosheets, the penetration depth is around 11-23 layers, which is dependent on the proton kinetic energy [3]. In the case of transition-metal dichalcogenides, H_2-filled bubbles were mainly located in the top interlayers [17]. Another method to induce H_2-filled bubbles is by decomposing trapped species. Electron-beam irradiation [18] and water electrolysis [19,20] were reported to be effective methods to dissociate intercalated

water molecules within 2D material layers. For example, with the help of electron-beam irradiation, large bubbles of up to 150×200 μm were induced in vacuum in h-BN film grown on sapphire substrate [18]. E-beam irradiation requires vacuum to induce h-BN bubbles, making it challenging to integrate with other experimental setups, such as testing h-BN's ability to act as a hydrogen proton exchange membrane in fuel cells. Therefore, in this work, we investigate a new approach for storing hydrogen gas inside h-BN bubbles upon exposure to a UV laser beam. This method holds promise as it does not alter the h-BN's surface stability; however, it affects the electronic properties of h-BN as it interacts with defects present in the material bulk. Indeed, it was shown that the doping nature and concentration in h-BN can be tuned using UV light [21]. The authors found that h-BN exhibited persistent photoconductivity lasting at least eight months, allowing a durable tuning of its conductivity. The study investigates the effect of illumination time on the size and density of h-BN bubbles by increasing the illumination from 5 to 480 min. It also studies the mechanism growth of h-BN bubbles through the aspect ratio var with the diameter. A mechanism of hydrogen formation inside h-BN upon UV illumination is proposed. The study uses AFM measurements to examine the stability of h-BN bubbles for four weeks and after six months. The physical properties, including internal pressure, number of top layers on h-BN bubbles, and storage capacities, are reported. This study demonstrates that h-BN bubbles created using UV laser light can be an efficient and stable system for hydrogen gas storage.

2. Results and discussion

2.1 Experimental characterization

The sample consists of 20 nm thick h-BN, which was grown on a 2 in. (0001) sapphire wafer using metal-organic chemical vapor deposition. Figure S1a shows Raman spectroscopy performed on the 20 nm h-BN sample. The spectrum is fitted with a Gaussian distribution that shows a peak at 1365 cm^{-1} attributed to the h-BN vibrational mode E_{2g} [22,23]. This latter is due to the in-plan vibrational mode of boron and nitrogen atoms which moves in opposite directions. The full-width at half maximum (FWHM) of the E_{2g} peak is around 49 cm^{-1}, which agrees with previous studies [22]. In our case, the FWHM is broader compared to the values reported in the literature for bulk h-BN (11.7 cm^{-1}) or few-layer h-BN flakes (15.6 cm^{-1}) [24]. The relatively broad peak obtained

here can be due to the spatial strain variation in the layer. The non-uniform strain can split the E_{2g} peak as observed for other 2D materials [22,25–27], resulting in a broader peak.

Figure S1b shows a HR-XRD $2\theta - \omega$ scan of 20 nm h-BN on sapphire substrate. A clear symmetric diffraction peak is located at 25.7, corresponding to the diffraction modes of h-BN's (0002) crystal planes. AFM images of the sample's surface morphology reveal wrinkle formation attributed to the difference in thermal expansion coefficient mismatch between h-BN and sapphire (see Figure S1e). This difference leads to an accumulation of compressive thermal strain in h-BN during cooling down from growth to room temperature. This observation is consistent with SEM images in Figures S1c and S1d, showing wrinkle formation in h-BN. The observed wrinkles could serve as an indirect indicator of the high crystalline quality of the grown h-BN film. In addition, we have noticed the formation of h-BN bubbles after exposing the sample to e-beam irradiation, as reported previously by Binder et al. [18] (see Figure S2a and S2b). After removing the samples from vaccum, h-BN bubbles deflate under atmospheric pressure (see Figure S2c). This can be due to the high e-beam irradiation energy that leads to deep penetration of hydrogen ions inside h-BN monolayers. This creates flat, large bubbles with low deformation that easily deflate under atmospheric pressure. A 213 nm UV laser beam is then used to create h-BN bubbles under an atmospheric environment. It should be noted that SEM images are taken on a different sample from the same 2-inch wafer to avoid overlapping between h-BN bubbles created by the e-beam and those induced by the UV laser beam. Raman spectroscopy was performed on h-BN bubbles to evaluate the presence of hydrogen gas inside h-BN bubbles. Figure 1 shows Raman spectra recorded on three h-BN bubbles. In addition to sapphire peaks, two additional peaks are observed at 354 and 587 cm^{-1}, which are attributed to the vibrational modes S(0) and S(1) of hydrogen molecules [18,28,29].

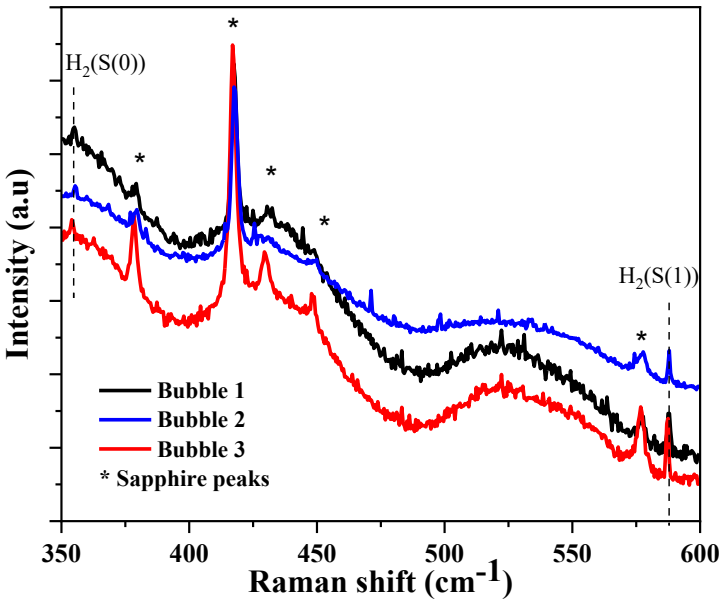

Figure 1. Raman spectroscopy of different h-BN bubbles, showing the vibrational modes S(0) and S(1) of H_2 molecule located at 354 and 587 cm^{-1}, respectively.

2.2 Statistical distribution of h-BN bubbles

The irradiation time of UV laser can significantly affect the density and size of h-BN bubbles. To understand the dependence of h-BN bubble size on illumination duration, we have investigated the effect of five illumination times: 5, 30, 60, 180, and 480 minutes, under atmospheric conditions. The effect of UV laser irradiation time on the density and size of h-BN bubbles is studied quantitatively and qualitatively through AFM scans and optical microscopy. Circular and crescent moon-shaped h-BN bubbles are obtained after illuminating the h-BN sample, as shown in

Figure **2** and Figure S3. The origin of crescent moon-shaped bubbles is unclear but can be due to non-uniformity in the adhesion energy between h-BN and sapphire substrate along the h-BN film. Additionally, the strain along the bubble membrane is higher at the center than at the edge. This is due to the bubble membrane's significant deformation, i.e., the bubble's curvature is high at the center. This can be attributed to the adhesion energy between h-BN and sapphire substrate that opposes the stretching of h-BN bubbles upon irradiation [30]. Seven AFM images were recorded on different regions of the illuminated spots for accurate statistics describing the total distribution of h-BN bubble size as a function of illumination time. Five of these AFM images are shown in Figure S4.

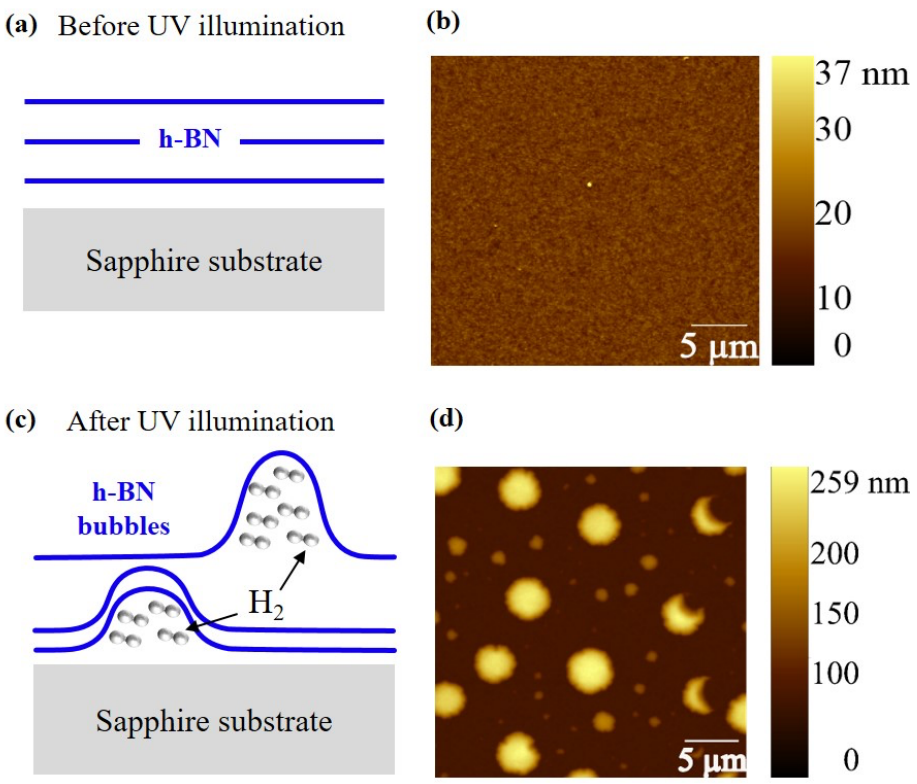

Figure 2. (a) Schematic illustration and (b) AFM image of h-BN on sapphire substrate. (c) Schematic illustration and (d) AFM image of h-BN on sapphire substrate irradiated by UV laser.

Figure S6 shows the distribution of h-BN bubble diameter as a function of the illumination time. The diameter of h-BN bubbles ranges from a few hundred nanometers to several micrometers. In addition, the diameter of these bubbles increases nearly five times from 5 minutes to 480 minutes of irradiation. The height distribution of h-BN bubbles also increases with the illumination time as shown in Figure S7. Figure 3a presents a histogram of the bubble density and the corresponding diameter for each illumination time. For ease of analysis, the diameter values have been sorted into four groups: $D \leq 1$ μm, 1 μm $\leq D \leq 3$ μm and 3 μm $\leq D \leq 6$ μm and $D \geq 6$ μm. As can be seen, the density of small bubbles ($D \leq 1$ μm) increases with the illumination time, indicating the ongoing creation of new bubbles. Furthermore, illuminating the sample for long durations results in big bubbles. In addition, when the illumination time increases from 30 to 60 min, the number of bubbles with 3 μm $\leq D \leq 6$ μm decreases, and new bubbles with $D \geq 6$ μm occur. Moreover, when the irradiation time increases from 180 to 480 min, the bubble density having 1 μm $\leq D \leq 3$ μm decreases, and new bubbles with 3 μm $\leq D \leq 6$ μm and $D \geq 6$ μm are created.

The reduction in bubble density when increasing the illumination time from 30 to 60 min and from 180 to 480 min can be attributed either to an increase in their size or a coalescence of small bubbles into bigger ones, as shown in AFM images (Figure S4a-e). Bubble coalescence is also observed in Figure S5, showing the optical images recorded on the same spot of the h-BN sample at different illumination times. As we illuminate the sample from 5 to 480 min, small bubbles merge into large ones. This can be attributed to the diffusion of hydrogen gas molecules from small bubbles to large ones, which is similar to the Ostwald ripening process [31,32].

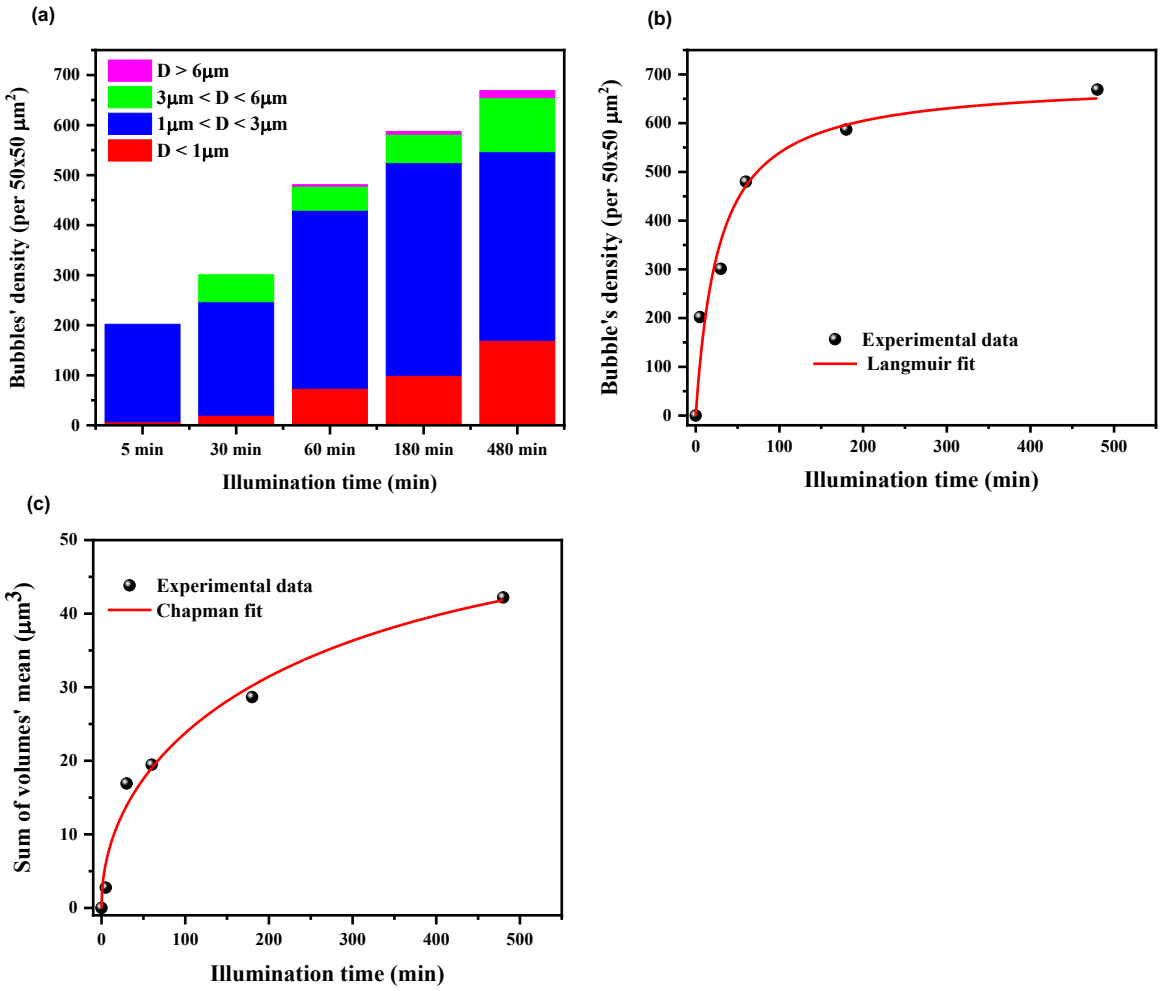

Figure 3. Influence of UV laser illumination time on h-BN bubble size. (a) Histogram of h-BN bubble density. (b) Variation of h-BN bubble density as a function of illumination time. (c) Total mean volume for each illumination duration as a function of illumination time.

Figure 3b illustrates the variation of bubble density (d_B (t)) per 50x50 µm^2 surface with illumination time. The density increases linearly and rapidly as the illumination time increases to 60 minutes. Then, it saturates for an illumination duration higher than 180 minutes. He et al. [7]

conducted a similar analysis and found that increasing hydrogen plasma treatment duration leads to larger bubbles with lower density. This can be attributed to a difference in bubble formation mechanism between the UV laser illumination and hydrogen plasma treatment. For the latter, the power and temperature of the plasma generator were 100 W and 350 °C, respectively. Such power and temperature lead to local heating of the h-BN bubbles and rapid diffusion of hydrogen gas molecules from small to large bubbles. In our case, h-BN bubbles are created at room temperature using a laser with power in milliwatts. This leads to a slow nucleation process of h-BN bubbles and almost constant bubble density, as evidenced by the results obtained for two days of illumination in Figure S5G. However, illuminating the sample for longer durations can result in lower bubble density due to their coalescence.

As shown in Figure 3b, the variation of bubble density as a function of illumination duration is well described by the Langmuir function: $\mathrm{d_B(t)} = \frac{\mathrm{d_m bt}}{1+\mathrm{bt}}$, where $\mathrm{d_m}$ is the maximum bubble density, and 1/b is the time needed to create half of the maximum bubble density. For example, to produce $d_m/2$ bubbles, the illumination time should be around 27 minutes.

Figure 3c shows the total mean volume, V_T, for each illumination as a function of time. The variation of V_T is well fitted by Chapman Richard's model as follows $V_T(t) = V_{max}(1 - \exp(-g_r t))^c$ [33]. This model was reported in the literature to study the growth of biological species (cells, molecules, etc). In this Equation, V_{max} is the maximum size of the bubble and g_r is the growth rate of bubbles when $V_T(t)$ increases from 0 to V_{max}. The dimensionless parameter c is equal to $\frac{1}{1-m}$, where m is the power exponent of volume size, and it determines the curve shape.

Table 1. Fitting parameters values used to model the bubble density, mean volume per bubble and total mean volume as a function of illumination time.

Physical parameter	Describing function	Fitting parameters
Bubble density per 50 x 50 μm^2	$\mathrm{d_B(t)} = \frac{d_m bt}{1+bt}$	$d_m = 688 \pm 57$ b = 0.036±0.012 min^{-1}
Total mean volume per 50 x 50 μm^2	$V_T(t) = V_{max}(1 - \exp(-g_r t))^c$	V_{max} = 50.92 ± 19.84 μm^3 g_r = 0.002 ± 0.003 min^{-1} c = 0.47 ± 0.17

2.3 Shape of h-BN bubbles

Figure 4 shows the height and aspect ratio variation of h-BN bubbles for each illumination. The height of h-BN bubbles increases linearly with the diameter, resulting in an aspect ratio h/R of 0.08. This aspect ratio implies a simultaneous increase in height and diameter because of the uniform H_2 pressure along the bubble membrane. The bubble dimensions increase until reaching an equilibrium value determined by the equilibrium between the elastic energy responsible for bubble stretching and the adhesion energy. This growth mechanism is responsible for the circular shape of h-BN bubbles. The average aspect ratio obtained from AFM measurements (h/R = 0.08) agrees closely with the aspect ratio (h/R = 0.11-0.14) reported in previous studies for circular bubbles [20,34]. The average strain of bubbles created in 2D materials is proportional to $\left(h/R\right)^2$ and it ranges between 1-2 % for monolayer graphene, h-BN, and MoS_2 bubbles [34–36]. In our case, for six layers on top of h-BN bubbles, the aspect ratio is 0.098 and the average strain is 0.96 %. The difference between our results and those reported in the literature can be due to the number of layers on top of h-BN bubbles.

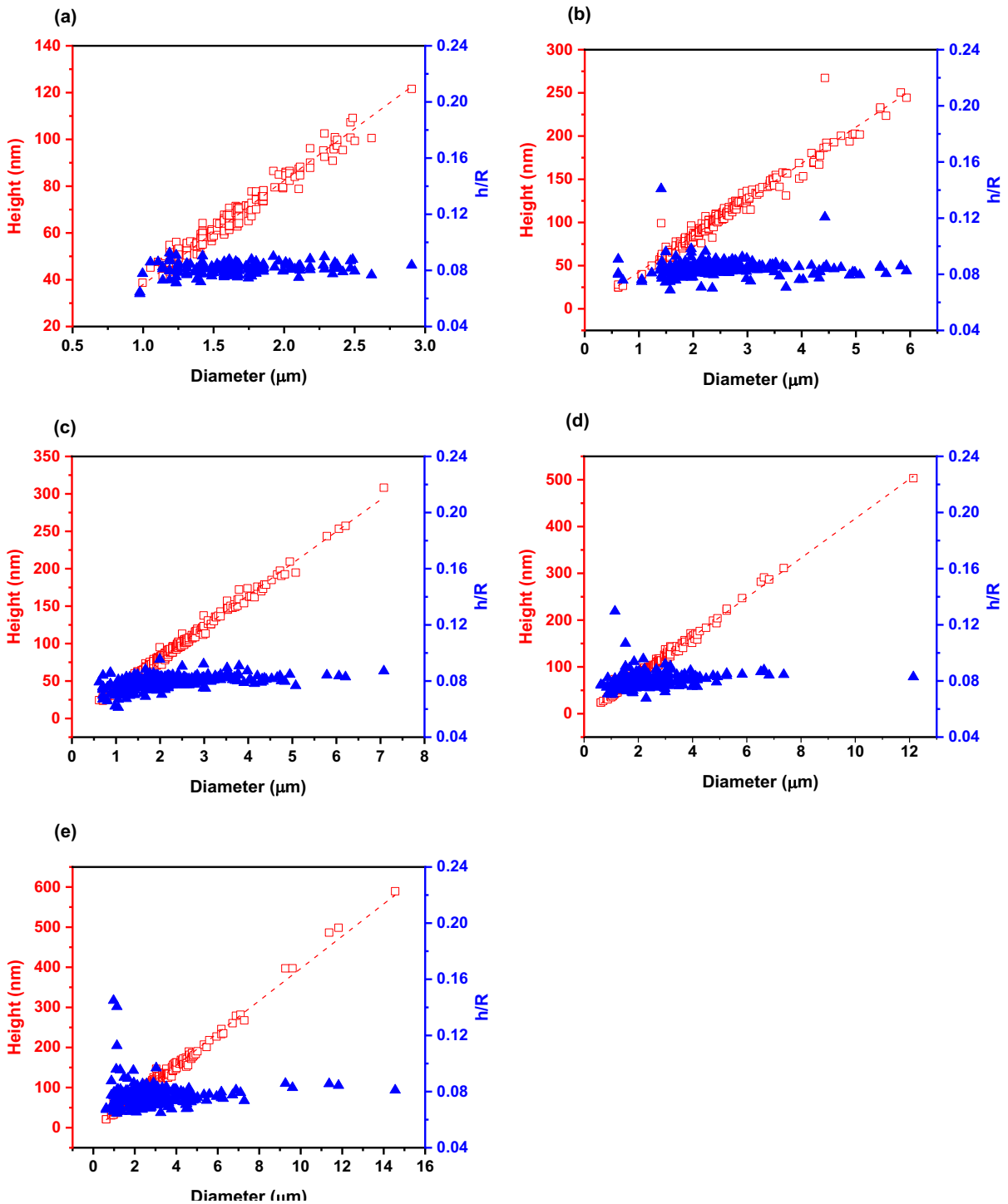

Figure 4. Variation of h-BN bubble height h and aspect ratio h/R after (a) 5 min, (b) 30 min, (c) 60 min, (d) 180 min, and (e) 480 min UV laser illumination.

2.4 Stability of h-BN bubbles

To investigate the stability of h-BN bubbles, we have recorded cross-sectional AFM profiles on three bubbles with a diameter and height equal to d = 27 µm, h = 1.1 µm (bubble 1), d = 10.9 µm, h = 434 nm (bubble 2) and d = 9.8 µm, h = 376 nm (bubble 3) (see Figure 5a,c,e). Figure 5d shows a reduction of 7% in the height of bubble 2 during the fourth week. As for bubbles 1 and 3, they exhibit a decrease of less than 1% (see Figure 5b,f). These results suggest that h-BN bubbles are stable and thus h-BN can be a promising system for hydrogen gas storage. In addition, bubble 1 has a height of 1100 nm, indicating the strong elasticity of h-BN film, whose thickness is only ± 20 nm. Additionally, AFM scans are performed on the same bubbles 1, 2, and 3 after six months of their formation (not shown in the study). We noticed no significant reduction in the dimensions of the bubbles. This suggests the high stability of h-BN bubbles, which can be a promising storage system for hydrogen.

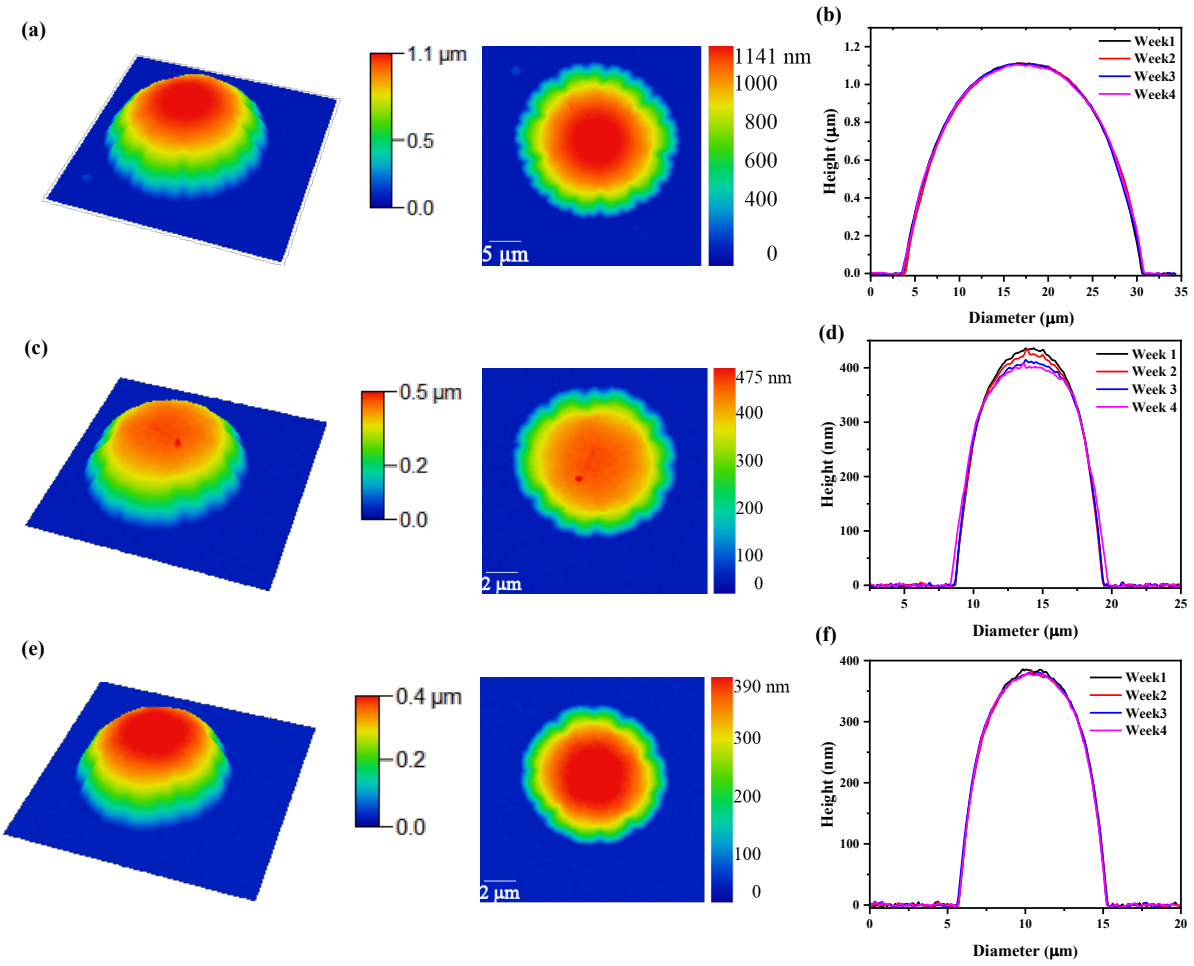

Figure 5. 3D and 2D AFM images of h-BN bubbles with (a) d = 27 μm and h = 1.1 μm, (c) d = 10.9 μm and h = 434 nm, and (e) d = 9.8 μm and h = 376 nm. (b, d, f) AFM cross-sectional profile of h-BN bubbles shown in (a, c, e), respectively.

2.5 Origin of hydrogen gas inside h-BN bubbles

To explain the origin of hydrogen gas confined inside h-BN bubbles, we consider that water vapor adsorbs and splits on vacant defects in h-BN. Water vapor molecules can break into N-H and B-OH bonds. Previous studies reported that water molecules split on defective h-BN and graphene films, forming B/C-OH and N/C-H bonds [37–39]. For example, Verma et al. demonstrated via molecular dynamic simulation that water molecule dissociates on vacancy defective h-BN nanosheets and that terminal nitrogen and boron atoms bond with a hydrogen atom and hydroxyl group, respectively [39]. The presence of vacancies in h-BN weakens the water molecule's bonding force, leading to its reorientation when it adsorbs on h-BN's surface (see Figure 6b). Because of the nitrogen atom's higher electronegativity than boron [40], nitrogen-water van der Waals attractions are stronger than boron-water attractions. This leads to the breakage of the H-O-H bond and the formation of H-N and OH-B bonds (Figure 6c). Because the energy of the 213 nm laser (5.8 eV) is higher than the bonding energy of O-H (4.8 eV) and N-H (3.91 eV), the sample irradiation induces a release of hydrogen atoms in these bonds (Figure 6d). The released hydrogen atoms recombine into H2 gas molecules and get trapped inside h-BN bubbles (Figure 6e,f). In addition, a 266 nm laser beam was used to create h-BN bubbles. Also, in this case, the formation of h-BN bubbles was observed. However, the process is sluggish compared to the 213 nm laser beam. This is consistent with our hypothesis, as the 266 nm laser having an energy of 4.66 eV can break only the N-H bonds. This leads to fewer h-BN bubbles, which require longer irradiation times to reach the same number as the 213 nm UV laser.

The ongoing process of h-BN bubble creation with illumination time can be explained by the formation of new vacancies due to UV laser light. This was reported in a previous study where h-BN irradiation with UV laser light induces nitrogen vacancies V_N [41]. The creation of new vacancies leads to new H_2 molecule formation and confinement inside h-BN bubbles. This process continues until all the adsorbed water molecules on the h-BN's surface are consumed leading to a saturation of h-BN bubble density, as illustrated in Figure 3b. Figure 6 summarizes the mechanism of hydrogen formation and confinement inside h-BN bubbles.

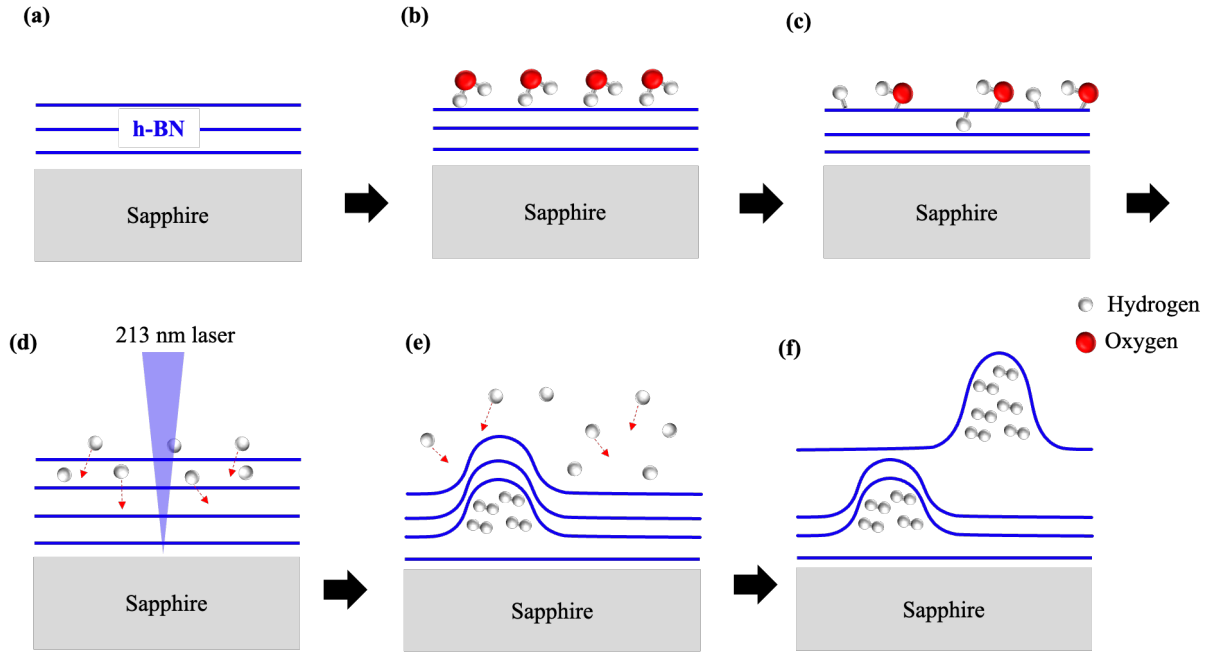

Figure 6. (a) h-BN film grown using MOCVD on sapphire substrate. (b) Adsorption of water molecule on h-BN nanosheets. (c) Dissociation of water molecules on vacancy sites in h-BN into N-H and OH-B bonds. (d) Sample exposure to 213 nm UV laser light. (e) Diffusion and recombination of hydrogen protons upon UV exposure. (f) Formation and confinement of hydrogen gas molecules inside h-BN bubbles.

2.6 Physical properties of h-BN bubbles

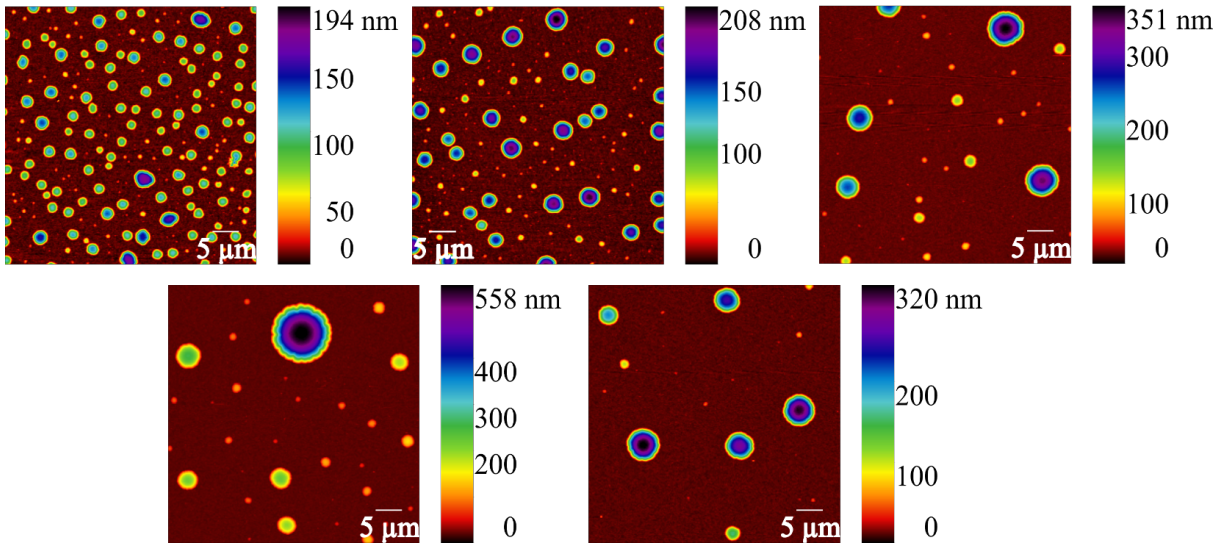

Figure 7. AFM images of h-BN bubbles for 180 min of illumination.

In order for h-BN bubbles to be useful in hydrogen gas storage applications, it is important to study their physical properties, including internal pressure and hydrogen storage capacity. To evaluate

these properties, we consider Yue et al. model, which assumes a uniform internal pressure within the bubbles and that the elastic strain energy is equivalent to the adhesion energy Γ between h-BN and the substrate [35]:

$$\Gamma = \frac{5\mathrm{Enth}^4}{8\phi(\nu)\mathrm{R}^4} \tag{1}$$

where n is the number of layers on top of h-BN bubbles, E is the Youngs modulus (0.85 TPa) of h-BN, t is the thickness (0.333 nm) of monolayer h-BN, h and R are the radius and height of bubbles, and $\phi(\nu)$ is the geometric prefactor, which is a function of Poisson's ratio $\nu = 0.2176$ [42–44] and is given by [19,35]:

$$\phi(\nu) = \frac{75\,(1-\nu^2)}{8(23+18\nu-3\nu^2)} \tag{2}$$

The height and radius of bubbles are measured from AFM measurements. The adhesion energy Γ is 0.32 J/m^2, as reported in [45].

By rearranging the terms of Equation (1), the number of atomic layers n on top of h-BN bubbles becomes:

$$\mathrm{n} = \frac{8\Gamma\phi(\nu)}{5\mathrm{Et}}\left(\frac{\mathrm{h}}{\mathrm{R}}\right)^{-4} \tag{3}$$

The number of top layers on h-BN bubbles, internal pressure, and storage capacity C are calculated for the bubbles shown in Figure 7. These images correspond to an illumination time of 180 min. We chose this illumination time for two reasons. First, it creates bubbles with dimensions similar to the other illumination times. Second, the density of h-BN bubbles saturates after 180 min, i.e., no remarkable change is observed in the size and density of bubbles. Figure 8a shows the number of layers n as a function of the aspect ratio h/R. n decreases with the increase of the aspect ratio. It drops from 25 to 10 layers when the aspect ratio is increased from 0.07 to 0.13. In addition, the variation of n with the diameter and height (see Figure S8a,b) suggests that small bubbles have more layers on top of them compared to large bubbles. The inset in Figure 8a shows that most of

the bubbles having an aspect ratio of 0.08, have 10-20 layers on top of them. This suggests that the majority of bubbles are formed at 3-6 nm below the h-BN surface.

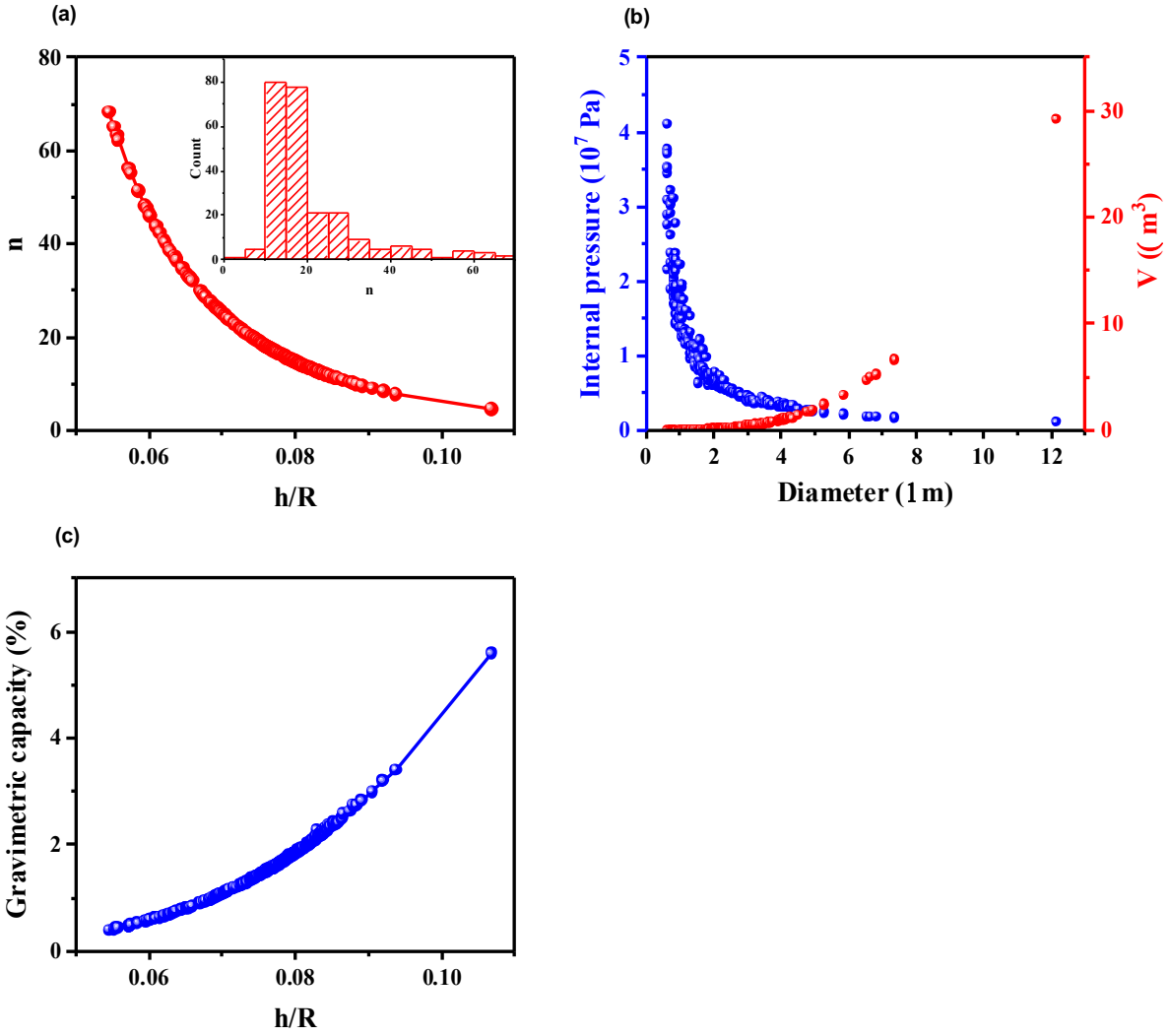

Figure 8. (a) The number of atomic layers on the top of h-BN bubbles as a function of aspect ratio h/R. (b) Variation of internal pressure and volume of h-BN bubbles versus the bubble diameter. (c) Hydrogen storage capacity C of h-BN bubble as a function of aspect ratio h/R.

The differential pressure Δp between the internal pressure inside the bubbles and the ambient external pressure is $\Delta p = p_{int} - p_{ext}$. Therefore, the internal pressure following Yue's model is [35]:

$$p_{int} = \frac{Enth^3}{\phi R^4} + p_{ext} \approx \frac{Enth^3}{\phi R^4} \quad (4)$$

By applying the ideal gas law, we obtain the number of hydrogen gas molecules N_G confined inside h-BN bubbles:

$$N_G = \frac{p_{int} V}{kT} \tag{5}$$

where k is the Boltzmann constant, T is the temperature and $V = \frac{\pi h}{6}(3R^2 + h^2)$ is the volume of h-BN bubbles (assuming spherical cap bubbles).

Figure 8b shows the internal pressure of h-BN bubbles and volume as a function of the diameter. For a bubble with a 618 nm diameter, the internal pressure and volume reach 41 MPa and 2.2×10^{-3} μm^3, respectively. As the diameter increases to 5 µm, the internal pressure decreases to 2.6 MPa while the volume increases to 1.94 μm^3. This indicates a higher internal pressure in small bubbles and a lower pressure in big bubbles.

The hydrogen storage capacity is computed to evaluate the ability of h-BN bubbles to store hydrogen gas. Assuming that hydrogen is the only gas confined inside h-BN bubbles. For a single h-BN bubble, the hydrogen storage capacity C is given by [46–48]:

$$C(\%) = \frac{2M_H N_G}{N_B M_B + N_N M_N + 2M_H N_G} \times 100 \tag{6}$$

where M_H is the molar mass of hydrogen, N_B, M_B and N_N, M_N are boron and nitrogen's number and molar mass in each h-BN bubble. Assuming that $N_B = N_N = N$, the number of boron and nitrogen atoms can be expressed as: $N = S/A_{uc}$, where $S = n\pi(R^2 + h^2)$ is the surface area of the h-BN bubble and $A_{uc} = 0.554\ nm^2$ is the area of the h-BN unit cell. The hydrogen storage capacity becomes:

$$C(\%) = \frac{2N_G A_{uc}}{S(M_B + M_N) + 2N_G} \times 100 \tag{7}$$

Figure 8c shows the variation in storage capacity, C, of h-BN bubbles as a function of the aspect ratio. The storage capacity increases to 5.9 % for an aspect ratio of 0.106. This suggests that large bubbles have a high storage capacity because of the high number of hydrogen molecules confined inside them (see Figure S9). For example, for a bubble with a diameter of 12 µm and height of 500 nm, the number of hydrogen molecules confined inside is 8×10^9 atoms. By comparing these results

with those obtained for n in Figure 8a, we notice that n and C exhibit an opposite trend variation with aspect ratio. This implies that thinner h-BN bubble membranes have a high gravimetric storage capacity. Table S1 summarizes the physical properties of h-BN bubbles with different dimensions.

To examine h-BN bubble properties, we can compare them with graphene nanobubbles created using water electrolysis reported in [19]. Hexagonal boron nitride (h-BN) bubbles and graphene nanobubbles exhibit distinct differences in their physical properties. For an h-BN bubble with a diameter and height of 0.99 μm and 35 nm, the number of top layers, internal pressure, and storage capacity are 25, 15 MPa, and 1.1 %, respectively. For a Graphene nanobubble with a 0.988 μm diameter and height of 106 nm, the number of layers, internal pressure, and storage capacity equal 123, 23.6 MPa, and 0.23 %. These results suggest that despite h-BN bubbles having fewer layers on top of them and lower internal pressure, they offer a higher hydrogen storage capacity than graphene nanobubbles. However, the higher internal pressure and greater number of layers in graphene nanobubbles could offer advantages in terms of structural stability under harsh conditions.

3. Conclusion

In this study, we have demonstrated the confinement of hydrogen inside h-BN bubbles induced using a UV laser from 20 nm h-BN grown on sapphire substrate. The confined hydrogen originates from water vapor adsorption, intercalation, and dissociation through h-BN monolayers. We have confirmed the presence of hydrogen gas molecules inside h-BN using Raman spectroscopy. This latter revealed the presence of H_2 vibrational modes S(0) and S(1) located at 354 and 587 cm^{-1}.

We have also shown using AFM that h-BN bubbles depend strongly on the illumination time. We obtain denser and bigger bubbles by increasing the illumination time from 5 to 480 minutes. The growth mechanism of these bubbles with illumination time indicates a simultaneous increase in diameter and height, resulting in an average aspect ratio (around 0.08). This also explains the bubbles' circular shape, which is governed by the equilibrium between elastic energy and adhesion energy between h-BN and substrate. We also investigated the stability of three bubbles with different sizes for four weeks using AFM. Their height cross-sectional profile remains constant. h-BN bubbles remain unchanged for more than six months after their creation.

Additionally, we explored the properties of h-BN bubbles, including internal pressure, number of top layers, and storage capacities. Our calculations revealed a maximum pressure of 41 MPa, which indicates the strong mechanical properties of these bubbles to endure such high pressure. We also found that gravimetric storage capacity is about 6 %, suggesting that h-BN bubbles can store high amounts of hydrogen gas. These results could support the development of new technologies based on 2D materials to produce and store green hydrogen gas.

4. Experimental section

Growth of h-BN film on sapphire

The sample consists of 20 nm h-BN grown on 2-inch (0001) sapphire wafer using MOCVD method. Triethylborane (TEB) and ammonia (NH3) were used as precursors for h-BN growth at temperatures around 1280°C in a hydrogen ambient at a pressure of 85 mbar.

Formation of h-BN bubbles

The h-BN bubbles were created using a 213 nm UV laser with an average power of 2 mW, a beam size of 269 microns, and a repetition rate of 1 kHz. Before illumination, the h-BN sample was exposed to atmospheric conditions by being mounted in a beaker upside down facing deionized water for 25 days at room temperature.

Characterization of h-BN bubbles

The sample's morphology was characterized by SEM, which was performed using Zeiss supra 55VP at EHT of 2.5 kV with SE2 detector. High-resolution X-ray diffraction (HR-XRD) scans were also performed in a Panalytical X'pert Pro Materials Research Diffractometer system using Cu Kα radiation (Cu Kα1 : 1.5405 Å) in the triple-axis mode.

AFM measurements were carried out using NX10 Park system under an ambient environment. The measurements were performed using contact mode with a PPP CONTSCR silicon probe. The cantilever has a length of 225 μm, a resonance frequency of 25 kHz and a spring constant of 0.2 N/m. The length and radius of the tip are 10 μm and 10 nm, respectively.

Raman measurements were performed on the Spectroscopy Platform of the LMOPS, Université de Lorraine & Centrale Supélec. The measurements were carried out using a Horiba Lab under an

atmospheric environment. The laser excitation wavelength is 532 nm with 100× objective. The laser spot size is 1 μm.

Statistical Analysis

Due to the challenge of performing AFM on the same illuminated spot, we irradiated different areas of the sample for durations of 5, 30, 60, 180, and 480 minutes. For each illumination time, seven AFM images were recorded. The bubble density was calculated by summing the number of bubbles found in each AFM scan. Similarly, the sum of volumes for each illumination time was determined by calculating the average total volume across the seven images.

Supporting Information

Supporting Information is available from the Wiley Online Library or from the author.

Acknowledgments

The authors would like to acknowledge funding from the French CNRS IRP ATLAS. The authors greatly acknowledge Dr. D. Chapron and Dr. T. H. Kauffmann from the Spectroscopy Platform of the LMOPS, Université de Lorraine & Centrale Supélec for their help with Raman measurements. The authors acknowledge Pascal Franchetti (LCP-A2MC) for technical assistance with the Raman measurements.

Received: ((will be filled in by the editorial staff))
Revised: ((will be filled in by the editorial staff))
Published online: ((will be filled in by the editorial staff))

References

[1] Z. Liu, Y. Gong, W. Zhou, L. Ma, J. Yu, J.C. Idrobo, J. Jung, A.H. Macdonald, R. Vajtai, J. Lou, P.M. Ajayan, Nat. Commun. 2013, 4, 1–8.

[2] F.Z. Tijent, P. Voss, M. Faqir, 2023, 33, 101275.

[3] L. He, H. Wang, L. Chen, X. Wang, H. Xie, C. Jiang, C. Li, K. Elibol, J. Meyer, K. Watanabe, T. Taniguchi, Z. Wu, W. Wang, Z. Ni, X. Miao, C. Zhang, D. Zhang, H. Wang, X. Xie, Nat. Commun. 2019, 10, 1–9.

[4] S. Hu, M. Lozada-Hidalgo, F.C. Wang, A. Mishchenko, F. Schedin, R.R. Nair, E.W. Hill, D.W. Boukhvalov, M.I. Katsnelson, R.A.W. Dryfe, I. V. Grigorieva, H.A. Wu, A.K. Geim, Nature 2014, 516, 227–230.

[5] S.I. Yoon, D.J. Seo, G. Kim, M. Kim, C.Y. Jung, Y.G. Yoon, S.H. Joo, T.Y. Kim, H.S. Shin, ACS Nano 2018, 12, 10764–10771.

[6] M. Seel, R. Pandey, 2D Mater. 2016, 3, 025004.

[7] L. Shi, A. Xu, G. Chen, T. Zhao, J. Phys. Chem. Lett. 2017, 8, 4354–4361.

[8] J. Shan, S. Fang, W. Wang, W. Zhao, R. Zhang, B. Liu, L. Lin, B. Jiang, H. Ci, R. Liu, W. Wang, X. Yang, W. Guo, M.H. Rümmeli, W. Guo, J. Sun, Z. Liu, Natl. Sci. Rev. 2022, 9.

[9] G. Constantinescu, A. Kuc, T. Heine, Phys. Rev. Lett. 2013, 111, 036104.

[10] T. Georgiou, L. Britnell, P. Blake, R. V. Gorbachev, A. Gholinia, A.K. Geim, C. Casiraghi, K.S. Novoselov, Appl. Phys. Lett. 2011, 99.

[11] E. Blundo, A. Surrente, D. Spirito, G. Pettinari, T. Yildirim, C.A. Chavarin, L. Baldassarre, M. Felici, A. Polimeni, Nano Lett. 2022, 22, 1525–1533.

[12] H.Y. Lee, S. Sarkar, K. Reidy, A. Kumar, J. Klein, K. Watanabe, T. Taniguchi, J.M. LeBeau, F.M. Ross, S. Gradečak, Nat. Commun. 2022,13, 1–9.

[13] X. Cui, L. Liu, W. Dong, Y. Zhou, Z. Zhang, Nano Research 2023,16, 13434-13449.

[14] W. Wang, X. Ma, Z. Dai, S. Zhang, Y. Hou, G. Wang, Q. Li, Z. Zhang, Y. Wei, L. Liu, c. 2022, 9, 2101939.

[15] Y. Hou, X. Ren, J. Fan, G. Wang, Z. Dai, C. Jin, W. Wang, Y. Zhu, S. Zhang, L. Liu, Z. Zhang, ACS Appl. Mater. Interface 2020, 12, 40958–40967.

[16] D.A. Sanchez, Z. Dai, P. Wang, A. Cantu-Chavez, C.J. Brennan, R. Huang, N. Lu, Proceedings of the National Academy of Sciences, 115, 7884–7889.

[17] D. Tedeschi, E. Blundo, M. Felici, G. Pettinari, B. Liu, T. Yildrim, E. Petroni, C. Zhang, Y. Zhu, S. Sennato, Y. Lu, A. Polimeni, D. Tedeschi, E. Blundo, M. Felici, E. Petroni, A. Polimeni, G. Pettinari, B. Liu, T. Yildrim, C. Zhang, Y. Zhu, Y. Lu, S. Sennato, Adv. Mater. 2019, 31, 1903795.

[18] J. Binder, A.K. Dabrowska, M. Tokarczyk, K. Ludwiczak, R. Bozek, G. Kowalski, R. Stepniewski, A. Wysmolek, Nano Lett. 2023, 23, 1267–1272.

[19] H. An, B.H. Tan, J.G.S. Moo, S. Liu, M. Pumera, C.D. Ohl, Nano Lett. 2017, 17, 2833–2838.

[20] S. Yasuda, K. Tamura, T.O. Terasawa, M. Yano, H. Nakajima, T. Morimoto, T. Okazaki, R. Agari, Y. Takahashi, M. Kato, I. Yagi, H. Asaoka, J. Phys. Chem. C 2020, 124, 5300–5307.

[21] A. Perepeliuc, R. Gujrati, A. Srivastava, P. Vuong, V. Ottapilakkal, P.L. Voss, S. Sundaram, J.P. Salvestrini, A. Ougazzaden, Appl. Phys. Lett. 2023, 122.

[22] X. Li, S. Sundaram, Y. El Gmili, T. Ayari, R. Puybaret, G. Patriarche, P.L. Voss, J.P. Salvestrini, A. Ougazzaden, Cryst. Growth Des. 2016, 16, 3409–3415.

[23] R. Geick, C.H. Perry, G. Rupprecht, Phys. Rev. 1966, 146, 543.

[24] L. Song, L. Ci, H. Lu, P.B. Sorokin, C. Jin, J. Ni, A.G. Kvashnin, D.G. Kvashnin, J. Lou, B.I. Yakobson, P.M., Nano Lett. 2010, 10, 3209–3215.

[25] J. Sun, C. Lu, Y. Song, Q. Ji, X. Song, Q. Li, Y. Zhang, L. Zhang, J. Kong, Z. Liu, Chem. Soc. Rev. 2018, 47, 4242–4257.

[26] W. Paszkowicz, J.B. Pelka, M. Knapp, T. Szyszko, S. Podsiadlo, Appl. Phys. A Mater. Sci. Process 2002, 75, 431–435.

[27] K.K. Kim, A. Hsu, X. Jia, S.M. Kim, Y. Shi, M. Hofmann, D. Nezich, J.F. Rodriguez-Nieva, M. Dresselhaus, T. Palacios, J. Kong, Nano Lett. 2012, 12, 161–166.

[28] D.K. Veirs, G.M. Rosenblatt, J. Mol. Spectrosc. 1987, 121, 401–419.

[29] A. Campargue, S. Kassi, K. Pachucki, J. Komasa, Phys. Chem. Chem. Phys. 2011, 14, 802–815.

[30] D.A. Sanchez, Z. Dai, N. Lu, Trends Chem. 2021, 3, 204–217.

[31] P. Taylor, Ostwald ripening in emulsions, Adv. Colloid Interface Sci. 1998, 75, 107–163.

[32] M. Ohring, M. Materials science of thin films: depositon and structure, Elsevier, 2001.

[33] L. Zhao-gang, L. Feng-ri, J. Forestry Research 2003, 14, 19–26.

[34] E. Khestanova, F. Guinea, L. Fumagalli, A.K. Geim, I. V. Grigorieva, Nat. Commun. 2016, 7.

[35] K. Yue, W. Gao, R. Huang, K.M. Liechti, J. Appl. Phys. 2012, 112.

[36] P. Wang, W. Gao, Z. Cao, K.M. Liechti, R. Huang, J. Appl. Mechanics 2013, 80, 040905.

[37] M.K. Kostov, E.E. Santiso, A.M. George, K.E. Gubbins, M.B. Nardelli, Phys. Rev. Lett. 2005, 95, 136105.

[38] A. Politano, A.R. Marino, V. Formoso, G. Chiarello, AIP Adv. 2011, 1.

[39] A. Verma, W. Zhang, A.C.T. Van Duin, Phys.Chem. Chem. Phys. 2021, 23, 10822–10834.

[40] C.Y. Won, N.R. Aluru, J. Am. Chem. Soc. 2007, 129, 2748–2749.

[41] L. Museur, D. Anglos, J.P. Petitet, J.P. Michel, A. V. Kanaev, J. Lumin. 2007, 127, 595–600.

[42] Q. Peng, W. Ji, S. De, Comput. Mater. Sci. 2012, 56, 11–17.

[43] K.N. Kudin, G.E. Scuseria, B.I. Yakobson, Phys. Rev. B 2001, 64, 235406.

[44] L. Song, L. Ci, H. Lu, P.B. Sorokin, C. Jin, J. Ni, A.G. Kvashnin, D.G. Kvashnin, J. Lou, B.I. Yakobson, P.M. Ajayan, Nano Lett. 2010, 10, 3209–3215.

[45] H. Rokni, W. Lu, Nat. Commun. 2020, 11.

[46] T. Tang, Y. Tang, Int. J. Hydrogen Energy 2024, 61, 13–24.

[47] D.P. Rai, B. Chettri, P.K. Patra, S. Sattar, ACS Omega 2021, 6, 30362–30370.

[48] I. Cabria, Int. J. Hydrogen Energy 2021, 46, 12192-12205.